IV.C.12 Improving the Kinetics and Thermodynamics of $Mg(BH_4)_2$ for Hydrogen Storage

Brandon Wood (Primary Contact),
Lennie Klebanoff, Vitalie Stavila, Tae Wook Heo,
Keith Ray, Jonathan Lee, Alex Baker,
ShinYoung Kang, Hui-Chia Yu, Katsuyo Thornton
Lawrence Livermore National Laboratory
7000 East Ave., L-413
Livermore, CA 94550
Phone: (925) 422-8391
Email: brandonwood@llnl.gov

DOE Manager: Jesse Adams
Phone: (720) 356-1421
Email: Jesse.Adams@ee.doe.gov

Subcontractors:
- Sandia National Laboratories (SNL), Livermore, CA
- University of Michigan, Ann Arbor, MI

Project Start Date: August 1, 2014
Project End Date: September 30, 2017

Overall Objectives

- Combine theory, synthesis, and characterization across multiple scales to understand the intrinsic kinetic and thermodynamic limitations in $MgB_2/Mg(BH_4)_2$.
- Construct and apply a flexible, validated, multiscale theoretical framework for modeling (de)hydrogenation kinetics of the Mg-B-H system and related metal hydrides.
- Devise strategies for improving kinetics and thermodynamics through nanostructuring and doping.

Fiscal Year (FY) 2017 Objectives

- Synthesize and test hydrogenation in unconfined MgB_2 nanoparticles.
- Compute free energies and validated phase diagram for the Mg-B-H system.
- Investigate mechanisms of initial and deeper MgB_2 hydrogenation.

Technical Barriers

This project addresses the following technical barriers from the Hydrogen Storage section of the Fuel Cell Technologies Office Multi-Year Research, Development, and Demonstration Plan.

(O) Lack of Understanding of Hydrogen Physisorption and Chemisorption

(A) System Weight and Volume

(E) Charging/Discharging Rates

Technical Targets

This project is conducting fundamental studies of hydrogenation and dehydrogenation of nanoscale $Mg(BH_4)_2$-based materials using a combined theory and experiment approach. Insights will be applied toward the design and synthesis of hydrogen storage materials that meet the following DOE hydrogen storage targets.

- Specific energy: 1.8 kWh/kg
- Energy density: 1.3 kWh/L
- Minimum delivery pressure: 5 bar
- Minimum delivery temperature: 85°C
- System fill time: 1.5 kg H_2/min

FY 2017 Accomplishments

- Computed and validated reference phase diagram of Mg-B-H including explicit thermal effects.
- Predicted that nanosizing/confinement affects reaction stability and pathway.
- Refined synthesis procedure for clean and pure unconfined MgB_2 nanoparticles.
- Demonstrated ~3x lower barriers in the initial uptake kinetics of unconfined MgB_2 nanoparticles with respect to bulk.
- Determined energy landscape for a two-step mechanism of initial hydrogen uptake in MgB_2 determined from X-ray and vibrational spectroscopy.
- Devised and applied a kinetic model for validation of the proposed two-step MgB_2 hydrogen uptake mechanism.
- Performed first full phase-field kinetics simulation of cycling between $MgB_{12}H_{12}$ and MgB_2, suggesting the possibility of different pathways for rehydrogenation and dehydrogenation in the hydrogen-poor domain.

INTRODUCTION

$Mg(BH_4)_2$ is one of very few metal hydride candidates that lie close to the "viability window" of capacity (14.9 wt% H) and desorption enthalpy (ΔH_{des}) required to satisfy the 2020 and ultimate DOE hydrogen storage targets [1–2]. However, $Mg(BH_4)_2$ suffers from extremely poor kinetics whose origin is not well understood. If the kinetic limitations could be removed and the effective ΔH_{des} slightly improved, then facile hydrogen uptake and release could be attained, and a complex metal hydride-based system could achieve long-term targets. Prior work points to particle size reduction and doping with additives as viable and cost-effective improvement strategies [3]. However, it is difficult to fully leverage these without comprehending how, why, and under what conditions these improvements are observed. This project applies multiscale theoretical and experimental tools to develop a fundamental understanding of kinetic and thermodynamic limitations in the Mg-B-H hydrogen storage system, and to devise specific strategies for optimizing its performance under cycling conditions.

APPROACH

This project aims to establish a closely coupled theory–characterization–synthesis approach to understand the roles of nanostructuring and doping in the Mg-B-H system, and apply it to devise possible strategies for improving kinetics and thermodynamics. We focus on three objectives: (1) identifying chemical, phase nucleation, or transport processes and determining which are rate limiting, (2) understanding the origin of the kinetic and thermodynamic changes upon nanosizing and doping, and (3) devising and implementing rational modifications for improvement of H_2 storage properties. Our modeling effort relies on the application of a multiscale framework that combines atomistic density functional theory (DFT) for predictive chemistry and thermodynamics with continuum phase-field modeling for describing phase nucleation and growth and non-equilibrium transport kinetics. The predictions are informed and validated by controlled synthesis of size-selected nanoparticles free from binders and nanoscaffolds that may otherwise burden the system with unacceptably high gravimetric penalties. To better understand the kinetic pathways and processes, we apply gravimetric and thermochemical analysis, and utilize in situ and ex situ microscopy and spectroscopy aided by computational interpretations to derive chemical and phase compositions. Particular emphasis is placed on understanding kinetic factors governing the rehydrogenation of MgB_2, which is generally less well understood than dehydrogenation.

RESULTS

MgB_2 Nanoparticle Synthesis & Characterization

To isolate mechanisms associated with nanosizing independently of confinement, we need doped and undoped nanoparticles of MgB_2 that are freestanding without a confining medium. This year, effort was directed to establishing a set procedure that allows the production of nanoparticles via surfactant ball milling without contamination from the milling hardware, surfactants, or solvents. We ball milled commercial MgB_2 using tungsten carbide milling hardware for 20 h in the presence of oleic acid and oleyl amine surfactant (stainless steel balls were previously found to introduce significant iron contamination). We found that tungsten carbide contamination could be minimized by interrupting the milling after 10 h, removing and replacing the balls under the glove bag, and continuing to mill for another 10 h. Next, we performed centrifugal separation of the product taken up in heptane (at 5,000 rpm for 25 min), with no supernatant observed. This material was washed three times with ethanol, consisting of adding ethanol to the deposit, ultrasonicating for 10 min, and centrifuging at 5,000 rpm for 25 min with decanting of the ethanol/surfactant solution. The deposit was dried overnight, then taken up in heptane and driven through a 100 nm Teflon filter. Transmission electron microscopy images confirmed that most of the particles we produced were <50 nm in diameter.

We used a combination of Fourier transform infrared spectroscopy (FTIR) and X-ray absorption spectroscopy (XAS) to confirm the purity of the particles. Figure 1 shows these tests for a particle using a 200 nm filter. In Figure 1a, FTIR was used to verify that the material is free of the surfactants (oleic acid, oleyl amine), the solvents used in the nanoparticle dispersal (heptane) and collection (ethanol), and oxidation. No signatures of the any of the dominant infrared-active frequencies are visible in the MgB_2 nanoparticles. The lack of significant oxide or nitride contaminants (MgO, Mg_3N_2) from air or moisture exposure was also confirmed by comparing against standards using Mg K-edge XAS, confirming the suitability of our sample handling procedures. Additional elemental analysis confirmed a lack of N or significant amounts of H. Some residual ~5 mole% carbon contamination was observed, but the carbon was unaffected by hydrogenating the MgB_2 sample at 140 bar H_2 and 365°C for 120 h.

Figure 1b shows the Sieverts uptake isotherm for hydrogenation of our unconfined nano-MgB_2 samples at 365°C and 140 bar H_2 pressure. The improvement in uptake kinetics is immediately visible. (Note that the decrease in total sample wt% H in the Sieverts data is likely due to the presence of residual surfactant, as these samples were extracted and tested prior to our refinement of the cleaning procedure described above.) A better idea of the kinetics can

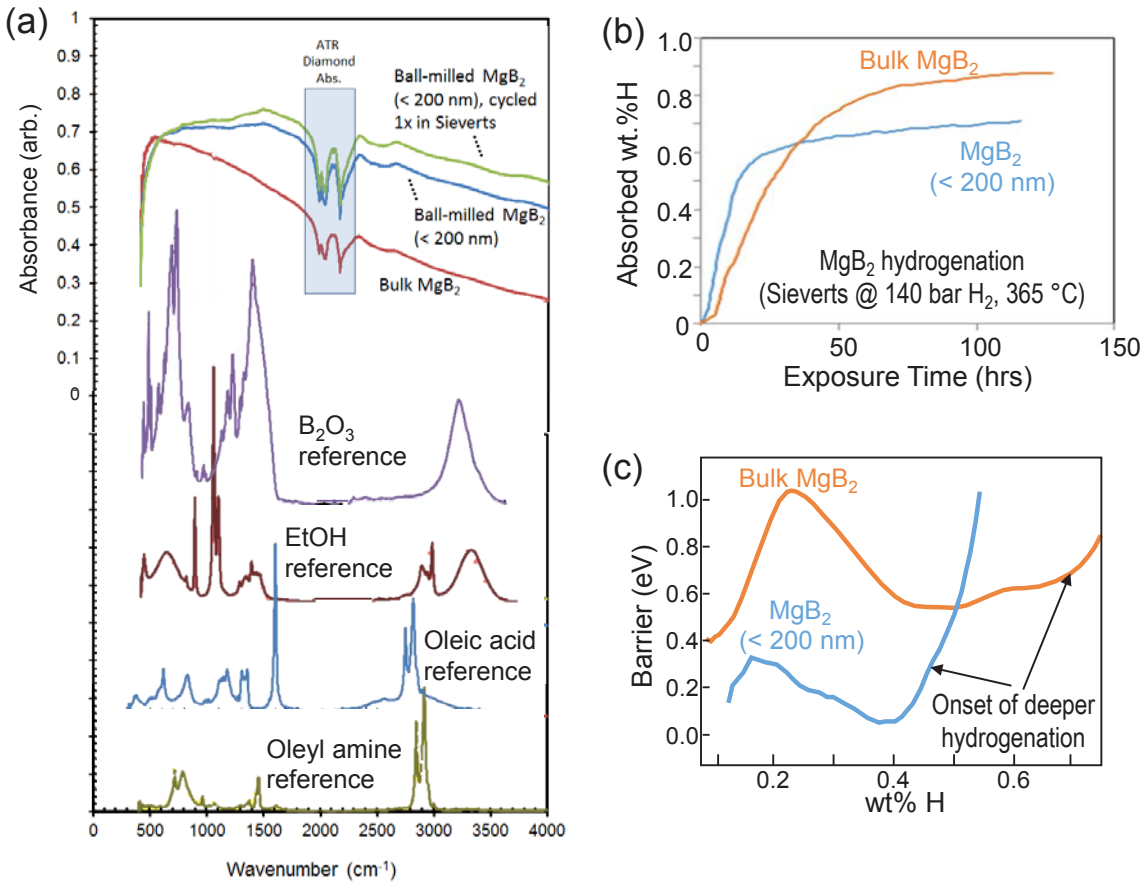

FIGURE 1. (a) FTIR spectra of nano-MgB_2 prepared according to the procedure described in the text (as-prepared and cycled). Spectra for bulk MgB_2 and possible contaminants from solvents or exposure to air are shown for comparison. (b) Sieverts initial hydrogen uptake in bulk MgB_2 and nano-MgB_2. (c) Evolution of the effective barrier during hydrogenation from Arrhenius analysis of the data in (b).

be gained by performing an Arrhenius analysis as a function of degree of hydrogenation. Following the procedure used in our recent work on understanding initial hydrogenation in bulk MgB_2 [4], we performed hydrogenation of nano-MgB_2 at two additional temperatures (378°C, 391°C) at 140 bar H_2 pressure. The resulting Arrhenius analysis is shown in Figure 1c. Similar to the bulk case, two barriers are observed in the initial hydrogenation regime. As described further in the sections below, the first corresponds to surface dissociation of H_2, whereas the second involves diffusion and binding to a lower-energy site. However, both barriers are dramatically reduced by ~3x upon nanosizing. Although these results clearly demonstrate the kinetic benefits of nanosizing, it should be emphasized that the Sieverts results can probe only the initial hydrogenation (<1 wt% H); the effect on the kinetics of the entire decomposition reaction has not yet been determined.

Free Energy Predictions for Mg-B-H

We computed free energies of the Mg-B-H compounds as a function of temperature (T) and H_2 partial pressure (pH_2), explicitly accounting for full finite-temperature dynamical contributions. Specifically, the solid vibrational density of states is computed from ab initio quantum molecular dynamics (based on DFT within the generalized gradient) and decomposed into (quasi)harmonic and anharmonic contributions. For these calculations, we have used the predicted structures in Zhang et al. [5] for $MgB_{12}H_{12}$. In principle, the predicted free energies can be used to construct a phase diagram for the conversion of $Mg(BH_4)_2$ to MgB_2 through the $MgB_{12}H_{12}$ solid-state intermediate. In doing so, we use the experimental entropy for hydrogen gas, as is standard practice in ab initio thermodynamics.

However, because DFT within standard approximations can mispredict reaction enthalpies, we first calibrated the temperature against pressure-composition-temperature (PCT) data in the literature from Li et al [6]. Although poor kinetics in the Mg-B-H system reduces the accuracy of PCT-derived thermodynamic data, the extracted values are nonetheless useful for approximate calibration. We found that a shift to higher temperatures by 280 K put the computations in good agreement with the PCT data. Note that this shift assumes that DFT errors in enthalpies are systematic, which is often the case. The calibrated $Mg(BH_4)_2$-$MgB_{12}H_{12}$-MgB_2

phase diagram based on ab initio molecular dynamics is shown in Figure 2a. By combining PCT measurement with transmission electron microscopy and selected area diffraction pattern, Li et al. observed the formation of MgH_2 at (360°C, 85 bar) and (285°C, 15 bar). [6] These points were used for temperature calibration of our phase boundary for the $Mg(BH_4)_2 \leftrightarrow 1/6\ MgB_{12}H_{12} + 5/6\ MgH_2 + 13/6\ H_2$ reaction. In addition, their X-ray diffraction analysis identified Mg metal at (360°C, 4.8 bar) formed from decomposition of MgH_2. This point resides close to our phase boundary between $1/6\ MgB_{12}H_{12} + 5/6\ MgH_2 + 13/6\ H_2$ and $1/6\ MgB_{12}H_{12} + 5/6\ Mg + 3\ H_2$, offering validation of our calibration choice.

To further validate our computed phase diagram, we have also been collaborating with the Hydrogen Materials—Advanced Research Consortium (HyMARC) to obtain the fraction of non-crystalline intermediate phases experimentally for $Mg(BH_4)_2$ and MgB_2 at different (pH_2,T) conditions. We have concentrated our validation efforts on the high-pressure end of the phase diagram, where the phase behavior is predicted to have higher sensitivity and where less data is generally available. ^{11}B nuclear magnetic resonance (NMR) is then used to estimate the fractions of MgB_2, $Mg(BH_4)_2$, and MgB_xH_y intermediates (mostly $MgB_{12}H_{12}$). These fractions can be compared against the predicted phase fractions from the free energy analysis.

NMR and X-ray diffraction (XRD) were used to obtain additional data points for samples obtained and hydrogenated through SNL/HyMARC and Pacific Northwest National Laboratory/HySCORE, as well as data published by Severa et al [7]. These analyses were performed around 400~550°C at various pressures up to 1,000 bar (marked with black, red, blue, and green circles in Figure 2a and identified in Figure 2c). Since the NMR and XRD data provide information about phase fractions, we also calculated the equilibrium phase fractions between $MgB_{12}H_{12}$ (as a broader stand-in for MgB_xH_y intermediates) and $Mg(BH_4)_2$ at 400–700°C close to the experimental conditions based on the phase coexistence approach we demonstrated previously [8]. While NMR and XRD data include kinetic effects, our phase diagram is solely based on thermodynamics. Therefore, direct comparison between the NMR/XRD-analyzed and our predicted phase fractions should be performed with caution. Nevertheless, the phase evolution trend found in NMR and XRD matches well with the trend in our predicted phase fractions, with higher levels of intermediates (or MgH_2 as a proxy for intermediates in XRD) appearing in regions near predicted phase boundaries, supporting our phase diagram prediction especially at higher (pH_2,T) conditions where the effect of anharmonic dynamics becomes dominant.

Kinetic Modeling of Initial MgB_2 Hydrogenation

As part of our ongoing investigation into the initial hydrogenation of MgB_2, we previously used a combination of

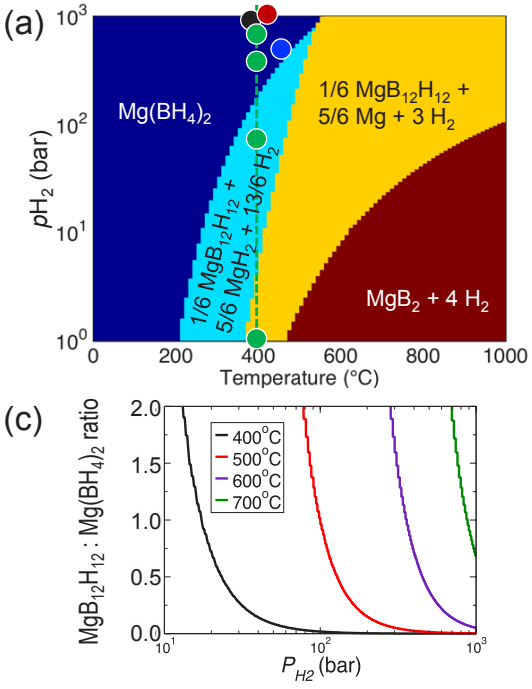

(b) **Experimental validation at high *P***

Sample	Method	T (°C)	pH_2 (bar)	Relative mole fractions of products (%)		
				MgB_xH_y	$Mg(BH_4)_2$	
Severa (2010)[1]	^{11}B NMR	390	900	7	93	
SNL #1	^{11}B NMR	420	1000	13	87	
SNL #2	^{11}B NMR	450	500	53	47	
				$Mg(BH_4)_2$	MgB_2	MgH_2
SNL/HyMARC #3 (White/Stavila)	XRD	400	1	75	25	0
		400	70	0	10	90
		400	350	66	34	0
		400	700	84	16	0

[1]Severa *et al.*, *Chem. Commun.* **46**, 421 (2010)

FIGURE 2. (a) Predicted and calibrated Mg-B-H phase diagram. (b) Details of experimental phase fractions measured under different conditions using ^{11}B NMR and XRD. The corresponding reaction conditions are shown as symbols in (a). (c) Calculated equilibrium phase ratio between $MgB_{12}H_{12}$ and $Mg(BH_4)_2$ for comparison with the experimental data in (b).

DFT calculations, FTIR, and XAS to suggest a two-barrier mechanism that is compatible with the barriers in Figure 1c. Ultimately, our proposed mechanism (shown in Figure 3a) leads to hydrogen segregation at high-energy B-B bonds of grain boundaries or interfaces and "etching" of the boron from these edge binding sites inward. In particular, this process involves successive chemical processes including H_2 molecule dissociation and adsorption of dissociated atomic H mediated by surface diffusion ("diffusive adsorption," hereafter) from the dissociation sites to the edge binding sites.

To verify and systematically analyze the proposed mechanism in Figure 3a, we devised a kinetic model that combines relevant non-equilibrium chemcial processes. We first constructed an energy diagram for the process in Figure 3a. The energetics of the proposed intermediates and products were computed from DFT, whereas the Arrhenius kinetic analysis of the experimental data in Figure 1c were used to parameterize the energy barriers of the corresponding chemical processes. The DFT calculations considered the coverage-dependent energy associated with binding hydrogen to exposed boron edge sites (the sites compatible with the XAS and FTIR results), as well as the dissociation energy of H_2 on Mg-rich planes of $MgB_2(0001)$. The resulting energy landscape is shown in Figure 3b.

Using the constructed energy diagram, a simple reaction rate law, and a well established isotherm model, we derived a mathematical model of reaction equations for the successive dissociation/association and diffusive adsorption/desorption processes. Our model couples differential equations for each of these two processes as follows. The overall reaction may be written as $H_2\,(g) \leftrightarrow 2H^* \leftrightarrow 2H_{ads}$, where H* represents hydrogen at the initial dissociation site and H_{ads} represents hydrogen bound to the edges of hexagonal boron in MgB_2. The set of differential equations can be written as:

$$\frac{\partial c_{H^*}}{\partial t} = k_1 \cdot P_{H_2} - \tilde{k}_1 \cdot c_{H^*}^2 - \frac{\partial c_H^{ads}}{\partial t}$$

$$\frac{\partial c_H^{ads}}{\partial t} = k_2 \cdot c_{H^*}^2 \cdot c_s^3 \cdot (1-\theta)^2 - \tilde{k}_2 \cdot c_s^3 \cdot \theta^2$$

Here, c_{H^*}, c_H^{ads} are concentrations of H^*, H_{ads}, respectively, in wt.% H, P_{H_2} is the pressure of H_2 gas, and θ is the edge binding site (adsorption site) coverage by adsorbed hydrogen. Note that c_H^{ads} and θ are related by $c_H^{ads} = f_{cv} N_s \theta$, where N_s ($= N_s^0 \cdot \exp(-E^{acc}/k_B T)$ is the number

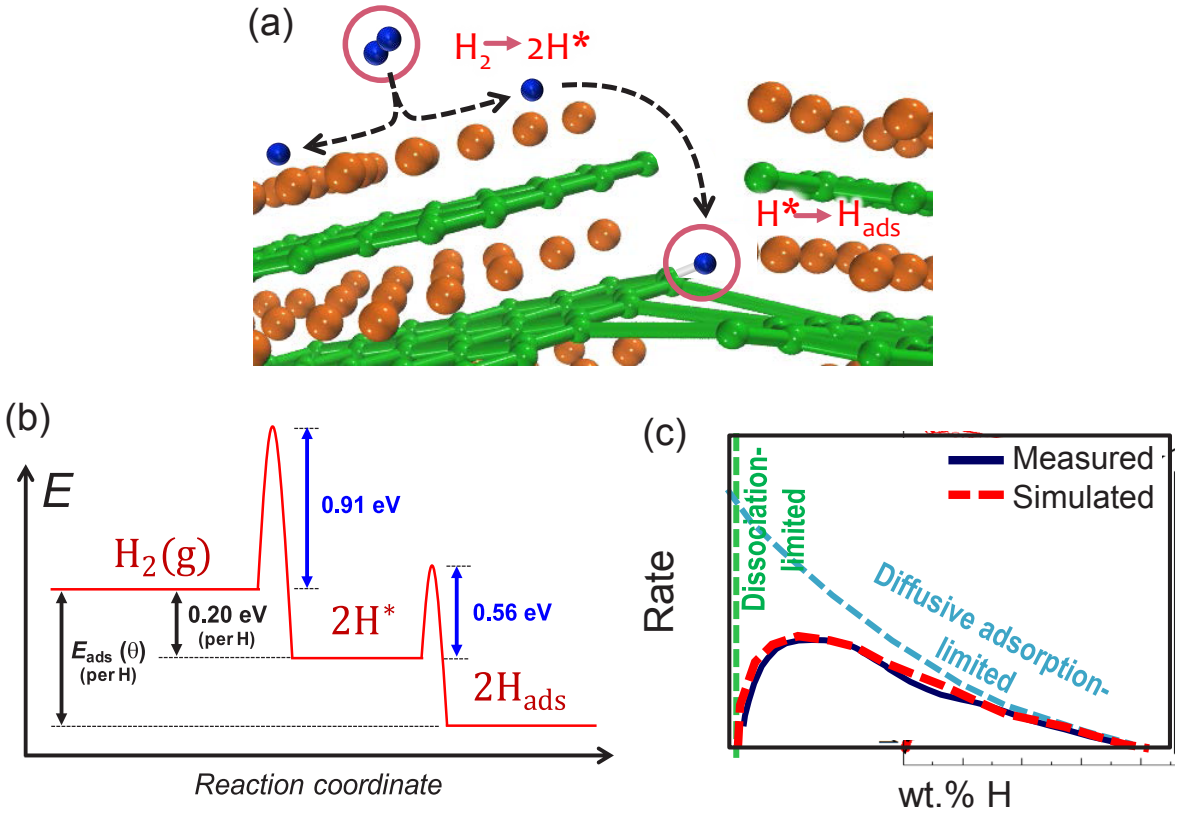

FIGURE 3. (a) Proposed mechanism of initial hydrogenation of MgB_2, involving dissociation ($H_2 \rightarrow 2H^*$) and diffusive adsorption ($H^* \rightarrow H_{ads}$) steps. (b) Corresponding energy diagram for the mechanism in (a). (c) Experimental and simulated uptake rate curves; results in the limit of a single-barrier rate limitation are also shown.

of accessible edge binding sites participating in adsorption and f_{cy} is the unit conversion factor to *wt.%* H. We define $c_s = c_s^0 \exp(-E^{acc}/k_BT)$ as the *effective* concentration parameter of the accessible edge binding sites, where c_s^0 is the corresponding prefactor and E_{acc} is the associated activation energy. The kinetic coefficients k_1, $\tilde{k}_1$, k_2, and $\tilde{k}_2$ correspond to dissociation, association, adsorption, and desorption, respectively. These kinetic coefficients are expressed in the form $k_0 \exp(-E^{acc}/k_BT)$, where k_0 is the prefactor, E is the activation energy, and k_B is the Boltzmann constant, and T is the temperature.

The above equations are numerically solved simultaneously to capture the interactions between the two processes. Note that this model contains some elements that are computed (e.g., DFT-derived energetics for different coverages), some that are measured (e.g., experimentally derived activation energies), and some that are purely descriptive (e.g., prefactors for the kinetic rate constants fitted to match simulated and experimental uptake curves). Our kinetic model can capture the significant mechanistic features, which allows us to verify our proposed initial hydrogenation mechanism. Figure 3c shows the simulated isotherm uptake curve versus the experimentally measured result, from which it is clear that the two-step mechanism reproduces the major kinetic features of the experimentally observed uptake. For more detailed analysis, we conducted controlled simulations for a particular temperature (T = 391°C) by manipulating the relative rates of the two operating reactions (dissociation/association and diffusive adsorption). Simulated rate curves for reactions limited entirely by dissocation/association (green dashed line) and entirely by diffusive adsorption (blue dashed line) are shown in Figure 3c. As expected, the blue line exhibits a monotonous decreasing trend with the increasing extent of hydrogenation due to the site saturation. In addition, it converges to the later stage of the fully relaxed simulation and experimental result (represented by red curves in Figure 3c). This manifests our above argument that the later-stage behavior of the rate curve is determined by the diffusive adsorption and site saturation processes. In contrast, the green line exhibits a monotonous increasing trend with the increasing the extent of hydrogenation. From this observation, we may further confirm that the very initial behavior of the uptake is determined by the dissociation/association reaction.

Phase-Field Kinetic Modeling

The kinetics of deeper rehydrogenation (>1 wt% H) in the hydrogen-poor region of the phase diagram are more difficult to probe, since they require higher temperatures that are inaccessible to our Sieverts apparatus. Instead, we performed phase-field kinetics simulations to qualitatively understand the relationship between diffusion, phase formation, and reaction pathways in the transformation between $MgB_{12}H_{12}$ and MgB_2. $MgB_{12}H_{12}$, MgB_4, MgB_2, and Mg were selected as the stoichiometric compounds for the hydrogen-poor region of the phase diagram (denoted Phase Triangle 3, the yellow region in Figures 4a and 4b). These compounds were proposed as possible intermediates by H.-W. Li et al [9]. The underlying free energy landscape was constructed based on our DFT-computed free energies at 350°C, with intermediate compositions interpolated using a mathematical smoothing function.

Multiphase phase field simulations were performed to examine the reaction pathways for rehydrogenation of MgB_2. In the simulations, a boundary condition corresponding to a high H chemical potential (i.e., high H_2 pressure) outside the particle is imposed to trigger the initial rehydrogenation. This allows the large nucleation barrier associated with

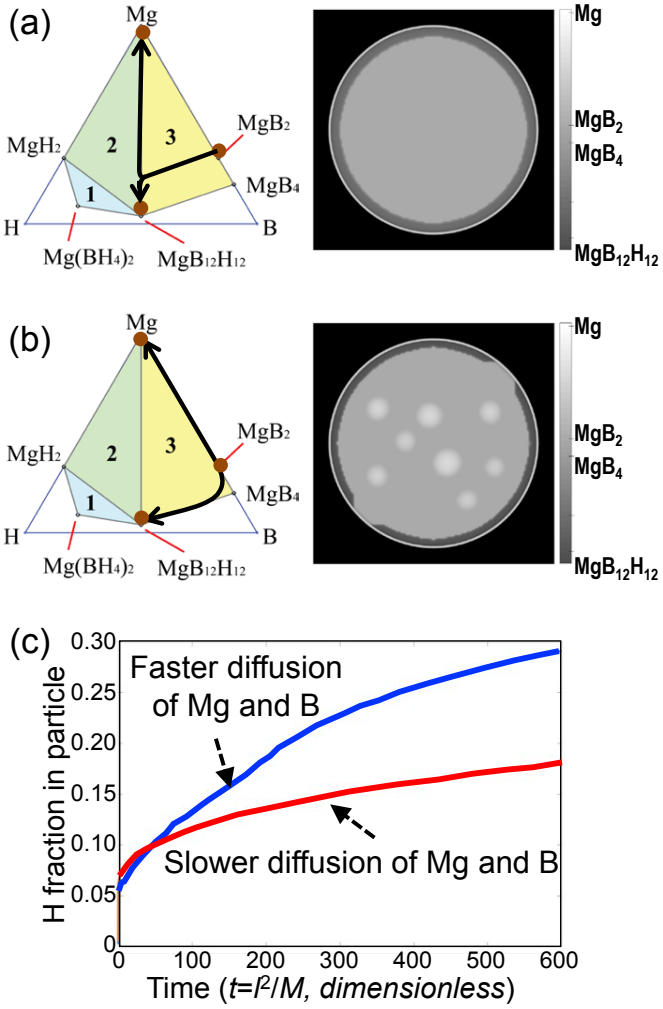

FIGURE 4. Simulated kinetic pathways and microstructure evolution during rehydrogenation of MgB_2 in the cases where (a) B and Mg mobilities are much smaller than H mobility (unitless mobilities: M_H = 0.01, M_B = M_{Mg} = 0.0001); and where (b) B and Mg mobilities are larger than H mobility (unitless mobilities M_H = 0.01, M_B = 1, M_{Mg} = 0.2). (c) Comparison of overall hydrogen uptake kinetics for the cases described in (b) and (b).

the initial insertion of H into MgB_2 to be overcome. Note that this barrier is associated with the steep gradient of the energy landscape near MgB_2 and suggests additives are necessary to catalyze B-B bond cleavage, as has been proposed. Figure 4a shows rehydrogenation simulation results if B and Mg mobilities are assumed to be sluggish compared to H mobility. As H is inserted into the particle, a core-shell morphology forms with a non-stoichiometric shell (the composition of which is approximately MgB_4H_4) and a core of MgB_2. The reaction pathway follows the pathway indicated in the left panel of Figure 4a; the low B and Mg mobilities hinder separation between these two species to form stoichiometric compounds and metallic Mg.

Another simulation was performed to examine the case when B and Mg mobilities are higher than H mobility (Figure 4b). Although this condition is unrealistic for bulk MgB_2, it represents a case for which B-B bond cleavage and Mg extraction are catalyzed. The result shows a very different morphological evolution from the previous one. As shown in Figure 4b, a $MgB_{12}H_{12}$ layer forms near the particle surface as H is inserted into the particle. As rehydrogenation proceeds, phases with high Mg concentration emerge from the MgB_2 region. Next, MgB_4 phases form and grow from the MgB_2 region. Meanwhile, the MgB_4 phases transform to $MgB_{12}H_{12}$, which grows with Mg inclusions. This composition evolution is indicated in the left panel of Figure 4b. The overall kinetics of hydrogen uptake from the two rehydrogenation simulations in Figures 4a and 4b are shown in Figure 4c. It is clear that faster Mg and B diffusion (as in Figure 4b) improves reaction kinetics, presumably because the composition evolution is allowed to occur via the low-energy pathways, i.e., from MgB_2 via MgB_4 to $MgB_{12}H_{12}$. Overall, the results in Figures 4 point to a close coupling between microstructure evolution, phase pathway, and (de) hydrogenation kinetics that merits further exploration.

CONCLUSIONS AND UPCOMING ACTIVITIES

This year, we refined our MgB_2 nanoparticle synthesis procedure and demonstrated the capability to make unconfined nanoparticles (MgB_2) without significant levels of contamination. The first tests of these materials were successfully made, showing significant kinetic enhancement for initial hydrogenation. The lack of a confining medium means the enhancement can be attributed exclusively to size effects. We also completed and validated a calibrated free energy-derived phase diagram for the transformation of $Mg(BH_4)_2$ to MgB_2 via a $MgB_{12}H_{12}$ intermediate. We further elucidated and verified a two-step kinetic mechanism for the initial hydrogenation of MgB_2, demonstrating the importance of interface reactions in determining the initial uptake kinetics of that material. Notably, the results suggest that introducing interfaces and/or defects will create additional reaction sites that should aid kinetics. Finally, we introduced the first phase-field kinetic model for probing the relative effect of Mg and B diffusion kinetics on the $MgB_{12}H_{12} \leftrightarrow MgB_2$ reaction pathway and rate. In the remaining months of the project, we will:

- Perform a more detailed analysis of the products and phase fractions of unconfined nano-MgB_2 in further detail, as well as of Ti-catalyzed samples of nano-MgB_2;
- Extend the phase-field model to the remaining region of the phase diagram (hydrogen-rich domain) and refine the energy landscape used as an input to the model.

FY 2017 PUBLICATIONS/PRESENTATIONS

1. B.C. Wood, V. Stavila, N. Poonyayant, T.W. Heo, K.G. Ray, L.E. Klebanoff, T.J. Udovic, J.R.I. Lee, N. Angboonpong, and P. Pakawatpanurut, "Nanointerface-driven reversible hydrogen storage in the nanoconfined Li-N-H system," *Adv. Mater. Interfaces* **4**, 1600803 (2017).

2. K.G. Ray, L.E. Klebanoff, J.R.I. Lee, V. Stavila, S. Kang, T.W. Heo, M. Bagge-Hansen, J. White, P. Shea, Y.-S. Liu, and B.C. Wood, "Elucidating the mechanisms of MgB_2 initial hydrogenation via a combined experiment-theory study," *Phys. Chem. Chem. Phys*., in press (2017).

3. B.C. Wood, "Complex dynamics in metal borohydrides: From hydrogen storage to solid-state batteries," Hydrogen Metal Systems Gordon Research Conference, Easton, MA, July 2017 [invited].

4. S. Kang, "Thermodynamics and Kinetics at Interfaces of Metal Hydrides for Hydrogen Storage," American Chemical Society Meeting, San Francisco, CA, March 2017.

5. S. Kang, "Beyond-ideal modeling of (de)hydrogenation in complex metal hydrides," International Symposium on Hydrogen Energy, Waikoloa, HI, February 2017 [invited].

6. K.G. Ray, "X-ray absorption and emission spectroscopy of the initial hydrogenation of MgB_2," Advanced Light Source User Meeting, Berkeley, CA, October 2016 [invited].

REFERENCES

1. Klebanoff, L.E., and J.O. Keller. "5 Years of Hydrogen Storage Research in the US DOE Metal Hydride Center of Excellence (MHCoE)." *Int. J. Hydr. Energy* 38 (2013): 4533–4576.

2. Pasini, J.M., C. Corgnale, B.A. van Hassel, T. Motyka, S. Kumar, and K.L. Simmons. "Metal hydride material requirements for automotive hydrogen storage systems." *Int. J. Hydr. Energy* 38 (2013): 9755–9765.

3. Fichtner, M., Z. Zhao-Karger, J. Hu, A. Roth, and P. Weidler. "The kinetic properties of $Mg(BH_4)_2$ in ltrated in activated carbon." *Nanotechnology* 20 (2009): 204029.

4. Ray, K.G., Klebanoff, L.E., Lee, J.R.I., Stavila, V., Kang, S., Heo, T.W., Bagge-Hansen, M., White, J., Shea, P., Liu, Y.-S., and Wood, B.C., "Elucidating the mechanisms of MgB_2 initial hydrogenation via a combined experiment-theory study," *Phys. Chem. Chem. Phys*., in press (2017).

5. Zhang, Y., Majzoub, E., Ozolins, V., and Wolverton, C., "Theoretical Prediction of Metastable Intermediates in the Decomposition of $Mg(BH_4)_2$." *J. Phys. Chem. C* 116 (2012): 10522.

6. Li, H.-W., Miwa, K., Ohba, N., Fujita, T., Sato, T., Yan, Y., Towata, S., Chen, M. W., and Orimo, S., "Formation of an intermediate compound with a $B_{12}H_{12}$ cluster: experimental and theoretical studies on magnesium borohydride $Mg(BH_4)_2$." *Nanotechnology* 20 (2009): 204013.

7. Severa, G., Rönnebro, E., and Jensen, C.M., "Direct hydrogenation of magnesium boride to magnesium borohydride: demonstration of >11 weight percent reversible hydrogen storage." *Chem. Commun.* 46 (2010): 421.

8. Wood, B.C., Stavila, V., Poonyayant, N., Heo, T.W., Ray, K.G., Klebanoff, L.E., Udovic, T.J., Lee, J.R.I., Angboonpong, N., and Pakawatpanurut, P., "Nanointerface-driven reversible hydrogen storage in the nanoconfined Li-N-H system," *Adv. Mater. Interfaces* 4 (2017): 1600803.

9. Li, H.-W., Yan, Y., Orimo, S., Züttel, A., and Jensen, C.M., "Recent Progress in Metal Borohydrides for Hydrogen Storage." *Energies* 4 (2011): 185–214.